Lenses on curved surfaces

R. C. Mitchell-Thomas,[1,*] O. Quevedo-Teruel,[2] T. M. McManus,[1] S. A. R. Horsley,[3] and Y. Hao[1]

[1]*School of Electronic Engineering and Computer Science, Queen Mary University of London, London E1 4NS, UK*

[2]*School of Electrical Engineering, KTH Royal Institute of Technology, SE-10044 Stockholm, Sweden*

[3]*Department of Physics and Astronomy, University of Exeter, Exeter EX4 4QL, UK*

**Corresponding author: r.c.mitchell-thomas@exeter.ac.uk*

Received March 6, 2014; revised May 12, 2014; accepted May 12, 2014;
posted May 14, 2014 (Doc. ID 206812); published June 9, 2014

This Letter presents a theory that allows graded index lenses to be mapped onto arbitrary rotationally symmetric curved surfaces. Examples of the Luneburg and Maxwell fish-eye lens are given, for numerous surfaces, always resulting in isotropic permittivity requirements. The performance of these lenses is initially illustrated with full-wave simulations utilizing a waveguide structure. A transformation of the refractive index profiles is then performed to design surface-wave lenses, where the dielectric layer is not only isotropic but also homogenous, demonstrating the applicability and ease of fabrication. © 2014 Optical Society of America

OCIS codes: (240.6690) Surface waves; (080.3630) Lenses; (220.2740) Geometric optical design.
http://dx.doi.org/10.1364/OL.39.003551

Rotationally symmetric graded index lenses [1–3], such as the Luneburg lens [4], are able to manipulate the ray paths so that, for example, an omnidirectional source can be transformed into a directive beam. These lenses have been implemented in parallel-plate and in three-dimensional systems in order to create directive antennas for microwave applications. They also have the advantage of being capable of beam steering, due to the rotationally symmetric structure, by changing the position of the source. Other graded index lenses include the Gutman lens [5], where the focal point can be shifted to a position either inside or at a distance from the surface of the lens, and the Maxwell fish-eye lens, that produces an image of the source on the far side of the lens [6].

These types of lenses have also been employed in the context of surface waves [7], utilizing metasurfaces [8] as the surface-wave-supporting structure. These devices have the advantage of being lightweight, thin, and low volume and are easier to fabricate when compared to their free-space equivalents. All of the current literature concentrates upon flat lens designs. However, if these lenses are to be used in microwave applications, it would be very advantageous for them to be conformal to an existing surface [9], particularly in the transport sector, where antennas can be attached to the outer surface of land or airborne vehicles without adversely affecting the aerodynamic properties [10]. This problem is the focus of this Letter, where lenses are modified so that they are accurate for curved surfaces. This allows for more freedom in terms of design parameters, ultimately leading to more efficient antennas [11].

It is known that surface curvature can alter the wave propagation across a surface. If we take the example of the surface of a sphere, all rays emitted from a point source on the surface will diverge away from that point, until they become parallel at the center, and then they begin to converge to create a perfect focus at the antipode. This behavior can be reproduced on a flat surface using a spherically symmetric refractive index profile, which in this case is the Maxwell fish-eye lens. In this Letter, both index profiles and curvature are combined to create lens behavior that is accurate on curved surfaces. In order to map an existing flat lens onto a rotationally symmetric curved surface, it is necessary to modify the refractive index profile. Figure 1 illustrates these two geometries, where the first is a flat space with a known rotationally symmetric graded index, and the second is an arbitrary rotationally symmetric curved surface. A standard cylindrical coordinate system is used, and the n_i labels are the refractive indices in the respective geometries. To retain the wave behavior of the first domain, a modified refractive index must be placed onto the second surface. This can be calculated by equating the ray paths on the two surfaces to give an equivalent optical length [2,12]. The ray paths in question are denoted in Fig. 1 with s_i and l_i labels. Equating the two s_i paths gives

$$n_1(r)2\pi r = n_2(\theta)2\pi R(\theta)\sin(\theta) \tag{1}$$

and the two l_i paths

$$n_1(r)dr = n_2(\theta)\sqrt{R(\theta)^2 + R'(\theta)^2}d\theta. \tag{2}$$

After finding the derivative of Eq. (1) and equating with Eq. (2), the following can be found:

$$\frac{n_2'(\theta)}{n_2(\theta)} = \frac{\left(1 + r\frac{n_1'(r)}{n_1(r)}\right)\sqrt{R(\theta)^2 + R'(\theta)^2} - R'(\theta)\sin(\theta) - R(\theta)\cos(\theta)}{R(\theta)\sin(\theta)}. \tag{3}$$

This equation can then be solved, either analytically or numerically, to find the modified index profile, $n_2(\theta)$.

To illustrate the accuracy of this technique, two example lenses are chosen, the Luneburg lens and the Maxwell fish-eye lens. These are mapped onto various surfaces, and the index required for each of these surfaces is shown in Fig. 2 for a lens with radius R_0. It can be seen that the required index contrast can be increased or decreased, depending on the type of surface. Also shown is a homogenous index for both lenses, which requires an "equivalent" surface to the lens, as previously reported

 © 2014 Optical Society of America

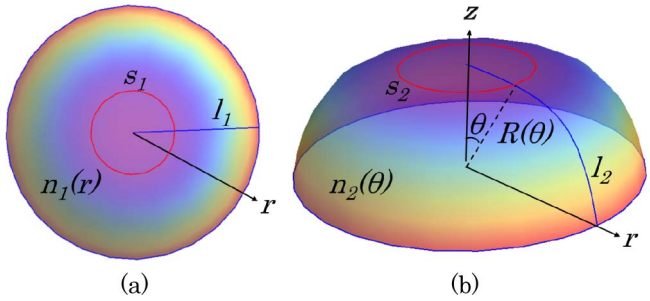

Fig. 1. Illustration of the ray paths that are equated for (a) the flat system and (b) an arbitrary rotationally symmetric curved surface. n_i is the refractive index on each surface.

[2,13]. In all these examples, it is possible to normalize the refractive index of the external surface, so the final device will only require refractive indices higher than 1.

In order to ensure that the waves are confined to a surface, it is possible to illustrate the operation of such devices using parallel-plate waveguides, where both plates follow the surface curvature but are separated by a tenth of the wavelength [14–16]. Figures 3 and 4 are simulated with COMSOL, with a perfect electric conductor (PEC) boundary condition for the upper and lower surfaces of the waveguide, and a perfectly matched layer (PML) is implemented around the edge. The E_z field component is then plotted at the upper surface of the waveguide. In Fig. 3, all four variations of the Luneburg lens shown in Fig. 2(a) are simulated, and they have been normalized so that the background index $n_0 = 3$. The first simulation, shown in Fig. 3(a), is a flat surface, where the usual Luneburg lens distribution, of the form $n_L = n_0\sqrt{2 - r^2}$, is employed. In Fig. 3(b), it is the equivalent surface that has been employed with a homogenous index. The required index for a Luneburg lens on a hemispherical surface can be calculated analytically and is given by $n_0\sqrt{1 + 3\cos\theta}/(1 + \cos\theta)^{3/2}$. This profile is simulated and shown in Fig. 3(c). A cosine shape is the final example, given in Fig. 3(d). The latter is chosen as any reflections due to the discontinuity where the curved part of the guide meets the flat, are removed [15], although it can be appreciated that this is not a major influence on the operation. It can be seen that all four simulations very accurately convert the cylindrical waves that are excited

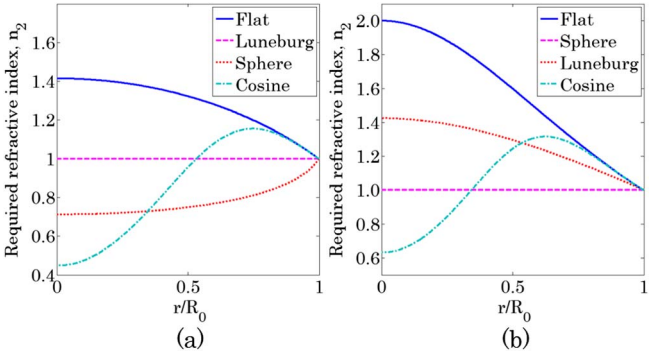

Fig. 2. Index profiles across a normalized lens radius, R_0, for (a) the Luneburg lens, and (b) the Maxwell fish-eye lens. Four surfaces are shown for each lens: the flat case, the Luneburg equivalent surface, the sphere case (Maxwell fish-eye-equivalent surface), and a cosine shape.

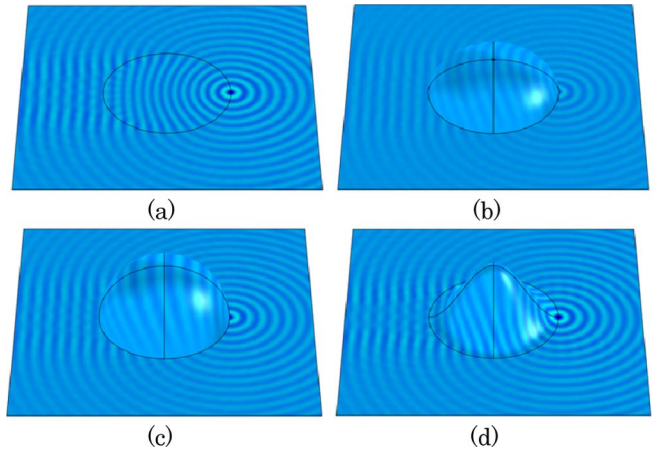

Fig. 3. Luneburg lenses with a radius of $5\lambda_0$, excited with a point source on the right edge of the lens, perfectly mapped onto four different surfaces: (a) a standard flat surface, (b) the equivalent homogeneous surface, (c) a hemispherical surface, and (d) a cosine surface.

by a point source at the outer edge of the device to a plane wave on the opposite side. Provided that these lenses are a sufficiently large number of wavelengths in diameter so that geometric optics holds, they can be scaled in both size and frequency.

The second example given here is the Maxwell fish-eye lens, which performs the function of forming a second focal point on the opposite side of the lens, when a point source is placed on the circumference. Again, the four profiles given in Fig. 2(b) are simulated, with a background index $n_0 = 3$. For a flat surface, it has a refractive index of $n_m = 2n_0/(1 + r^2)$, and this configuration is shown in Fig. 4(a). This lens is known to obtain the same wave propagation characteristics as a homogeneous hemispherical surface, and this is confirmed by the simulation in Fig. 4(b). In Fig. 4(c), it is the "Luneburg shape" that is chosen; however, here it is not homogenous but has the appropriate index, thereby obtaining the characteristics of the fish-eye lens, as illustrated in Fig. 2(b).

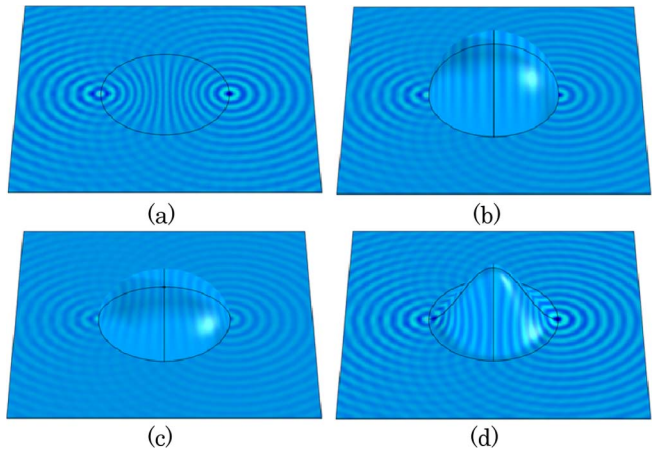

Fig. 4. Maxwell fish-eye lens with radius of $5\lambda_0$, excited with a point source on the right edge of the lens, perfectly mapped onto four different surfaces: (a) a standard flat Maxwell fish-eye lens, (b) the equivalent homogeneous surface (sphere), (c) an equivalent surface for a Luneburg lens, and (d) a cosine surface.

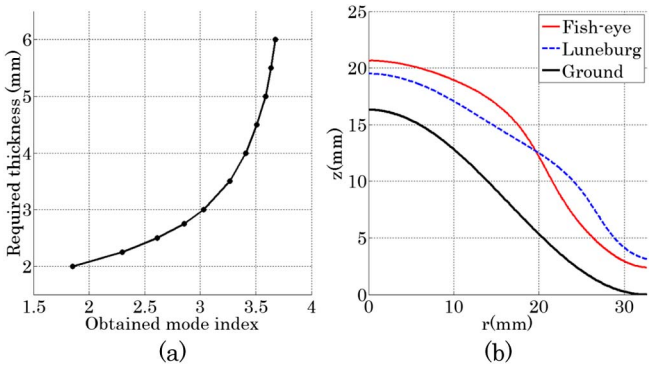

Fig. 5. (a) Achieved refractive index at 10 GHz of the surface for varying thickness of a dielectric slab with a permittivity of $\varepsilon_r = 15$ which is placed over a metallic surface. (b) Cross section of the required dimensions of the Luneburg and Maxwell fish-eye lenses above the cosine-shaped ground plane.

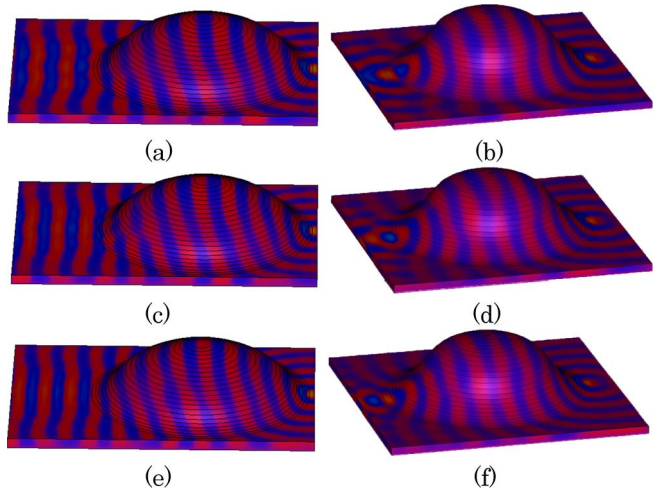

Fig. 6. Surface-wave propagation for the Luneburg (a), (c), (e) and Maxwell fish-eye lenses (b), (d), (f). All simulations have a cosine-shaped ground plane and a homogeneous dielectric overlayer of $\varepsilon_r = 15$ with a varying thickness. Frequencies are (a), (b) 10.5 GHz, (c), (d) 11 GHz, (e), (f) 11.5 GHz.

Finally, in Fig. 4(d), it is again the cosine shape that is chosen, giving a fourth example of this lens on a curved surface.

All of the previous simulations have utilized parallel-plate waveguides to illustrate the performance. One other option for these lenses is to implement surface-wave devices for leaky wave or end-fire antennas [17]. For these devices it is necessary to choose one of the possible surface-wave-supporting structures. These are either metasurfaces, which can be composed of an array of patches, or a dielectric slab over a ground plane. Here, the dielectric slab has been chosen, due to the simplicity with which it can then be fabricated. The varying refractive index is obtained by changing the thickness of a homogeneous dielectric slab over a metallic surface, in order to obtain the required mode index. An example is given in Fig. 5(a), where, for a dielectric with relative permittivity 15, the thickness of the slab is varied between 2 and 6 mm to give a range of mode indices at 10 GHz. This relation is then used to design two lenses. Both the Luneburg and the Maxwell fish-eye lens appropriate for the cosine-shaped surface are shown in Fig. 5(b). It can be appreciated that small changes in the shape of the dielectric overlayer can obtain quite differing propagation characteristics.

The two surface-wave lens designs shown in Fig. 5(b) were implemented in CST Microwave Studio, and the electric field component normal to the surface is plotted in Fig. 6. In both cases, the excitation of the structure is a point source positioned on the circumference of the lens, on the right of each figure. For the Luneburg lens, it can be observed that the omnidirectional source is transformed into a plane wave and therefore creates a directive beam propagating to the left. In the Maxwell fish-eye simulations, the new design is also successful in creating an image of the source on the right side of the lens. One thing to note is that although the lenses were designed for an operating frequency of 10 GHz, a shift of the optimal performance can be observed, to a slightly higher frequency. This is due to the fact that the theory assumes that the rays are perfectly confined to a surface. However, for the surface waves under consideration here, the waves are guided by the dielectric and are therefore not a perfect 2D system. Due to the curvature, the wave propagating further from the ground plane has a slightly longer path than that propagating closer to it, resulting in a small variation of the optimum frequency of operation from the design frequency of 10 GHz.

In summary, this Letter has proposed a technique to modify known radially dependant refractive index lenses so that they function accurately when mapped onto rotationally symmetric curved surfaces. Two examples of the Luneburg lens and the Maxwell fish-eye lens have been demonstrated for application onto various surface shapes and simulated using a dielectric-filled parallel-plate waveguide. To illustrate the application for surface-wave antennas, varying thickness dielectric lenses were designed and simulated, showing the accuracy of the technique. Due to the isotropy and homogeneity of these lenses, they are very simple to fabricate and could therefore prove to be of interest for antenna designs for improved communication systems.

This work was funded by the Engineering and Physical Sciences Research Council (EPSRC), UK, under a Program Grant (EP/I034548/1) “The Quest for Ultimate Electromagnetics using Spatial Transformations (QUEST).”

References

1. T. A. Rhys, IEEE Trans. Antennas Propag. **18**, 497 (1970).
2. M. Sarbort and T. Tyc, J. Opt. **14**, 075705 (2012).
3. M. Sarbort and T. Tyc, J. Opt. **15**, 125716 (2013).
4. R. K. Luneburg, *Mathematical Theory of Optics* (Cambridge University, 1964).
5. A. S. Gutman, J. Appl. Phys. **25**, 855 (1954).
6. U. Leonhardt, New J. Phys. **11**, 093040 (2009).
7. J. A. Dockrey, M. J. Lockyear, S. J. Berry, S. A. R. Horsley, R. J. Sambles, and A. P. Hibbins, Phys. Rev. B **87**, 125137 (2013).
8. S. Maci, G. Minatti, M. Casaletti, and M. Bosiljevac, IEEE Antennas Wirel. Propag. Lett. **10**, 1499 (2011).
9. X. Shen, T. J. Cui, D. Martin-Cano, and F. J. Garcia-Vidal, Proc. Natl. Acad. Sci. USA **110**, 40 (2013).
10. L. Josefsson and P. Persson, *Conformal Array Antenna Theory and Design*, IEEE Press Series on Electromagnetic Wave Theory (Wiley, 2006).

11. O. Quevedo-Teruel and Y. Hao, Opt. Lett. **38**, 392 (2013).
12. U. Leonhardt and T. G. Philbin, *Geometry and Light: The Science of Invisibility* (Dover Publications, 2010).
13. M. V. Berry, J. Phys. A **8**, 1952 (1975).
14. J. C. Minano, P. Benitez, and J. C. Gonzalez, New J. Phys. **12**, 123023 (2010).
15. R. C. Mitchell-Thomas, T. M. McManus, O. Quevedo-Teruel, S. A. R. Horsley, and Y. Hao, Phys. Rev. Lett. **111**, 213901 (2013).
16. S. A. R. Horsley, I. R. Hooper, R. C. Mitchell-Thomas, and O. Quevedo-Teruel, Sci. Rep. **4**, 4876 (2014).
17. D. R. Jackson, C. Caloz, and T. Itoh, Proc. IEEE **100**, 2194 (2012).

130.237.53.39 {ts '2017-08-04 13:09:47'}